Acute manipulation and real-time visualization of membrane trafficking and exocytosis in Drosophila

Jade Glashauser[1], Carolina Camelo[1], Manuel Hollmann, Jone Isasti Sanchez, Thea Jacobs, Wilko Backer, Dominique Förster[2] and Stefan Luschnig[*]

Institute of Integrative Cell Biology and Physiology, University of Münster, Badestrasse 9, D-48149 Münster, Germany

Cells in Motion (CiM) Interfaculty Center, University of Münster, D-48149 Münster, Germany

[1]: co-first authors

[2]: present address: Max Planck Institute of Neurobiology, D-82152 Martinsried, Germany

[*]**Correspondence:** luschnig@uni-muenster.de

Running title: Synchronized membrane trafficking *in vivo*

Keywords: Membrane trafficking, exocytosis, secretion, endoplasmic reticulum, Golgi apparatus, epithelium, tracheal system, tricellular junction, *Drosophila.*

Abstract

Intracellular trafficking of secretory proteins plays key roles in animal development and physiology, but essential tools for investigating the dynamics of trafficking have been limited to cultured cells. Here we present a system that enables acute manipulation and real-time visualization of membrane trafficking through reversible retention of proteins in the endoplasmic reticulum (ER) in living multicellular organisms. By adapting the “retention using selective hooks” (RUSH) approach to *Drosophila*, we show that trafficking of GPI-linked, secreted, and transmembrane proteins can be controlled with high temporal precision using streptavidin “hooks” and biotin-induced release in intact animals and cultured organs. We demonstrate the potential of this approach by analyzing the kinetics of ER exit and of apical secretion in tracheal tubes and the spatiotemporal dynamics of tricellular junction assembly in epithelia. Furthermore, hook-induced ER retention enables tissue-specific knockdown of secretory protein function. The system is compatible with available protein-traps and is widely applicable to investigate membrane trafficking in diverse cell types *in vivo*.

Introduction

A significant portion of genes in metazoan genomes encode secreted or membrane proteins (Meinken et al., 2015; Pei et al., 2018). The secretory apparatus ensures the correct delivery of these proteins to the extracellular space, the cell surface and intracellular membrane compartments, where they carry out a wealth of functions in cell adhesion, cell shape regulation, motility, and signaling during development and homeostasis. Accordingly, mutations in many secretory pathway components have been associated with developmental defects and diseases (Schotman and Rabouille, 2009; Yarwood et al., 2020).

While many insights into the organization and function of the secretory pathway were obtained in cultured mammalian cells and in yeast, which are amenable to biochemistry, genetics and imaging, analogous studies in intact multicellular organisms have been limited by the lack of adequate tools to manipulate membrane trafficking *in vivo*. Analyzing the dynamics of these processes is challenging, because sub-pools of a given protein species move simultaneously along multiple intracellular routes (synthesis, exocytosis, endocytosis, recycling, degradation) and localize in different membrane compartments, which cannot be separated at steady state. Therefore, the synthesis or transport of selected secretory proteins needs to be synchronized in order to follow their routes through the secretory apparatus. Classical methods for synchronizing secretory protein trafficking in cultured cells either rely on temperature blocks (Griffiths et al., 1985) or drugs (e.g., Brefeldin A; Lippincott-Schwartz et al., 1989) to reversibly arrest intracellular transport, or employ special conditionally mis-folded or aggregated proteins that are retained in the endoplasmic reticulum (ER), from where they are released by shifting cells to permissive temperature (Kreis and Lodish, 1986; Lafay, 1974) or by illumination with UV light (Chen et al., 2013). Although these approaches have revealed fundamental insights into the organization and dynamics of the secretory apparatus in cultured cells, they are limited to special proteins (e.g. the conditional thermosensitive viral glycoprotein VSVGtsO45; Kreis and Lodish, 1986) and require treatments using non-physiological temperatures, toxic agents, or potentially damaging doses of UV light.

A powerful experimental system that avoids these limitations is the '*retention using selective hooks'* (RUSH) system (Boncompain et al., 2012). RUSH enables synchronization of trafficking using a two component-system comprising (i) a secretory protein of interest tagged with a fluorophore and a streptavidin-binding peptide (SBP) and (ii) a streptavidin (SA) "hook" protein bearing a signal sequence that targets the protein to a membrane compartment of choice (*e.g*. a KDEL motif for retention in the ER). When cargo and hook constructs are co-expressed, they form a complex that is retained in the donor compartment in the absence of biotin (Fig. 1A). Addition of biotin rapidly dissociates the cargo-hook

complex and leads to release of cargo from the donor compartment, allowing to follow the synchronized trafficking of the fluorescent cargo molecules through the secretory apparatus. Importantly, RUSH is applicable to diverse cargo proteins, and their trafficking can be controlled at physiological temperatures using a non-toxic cell-permeable small molecule. This approach revealed important insights into the molecular events underlying ER exit (Shomron et al., 2021), ER-to-Golgi transport (Weigel et al., 2021; Westrate et al., 2020), intra-Golgi trafficking and transport of cargo between the Golgi apparatus and the plasma membrane (Fourriere et al., 2016; Stalder and Gershlick, 2020). However, applications of the RUSH system have thus far been limited to cultured cells, which typically do not represent the complexity of tissues in multicellular organisms, where membrane trafficking is developmentally or physiologically regulated.

We present here a set of tools that enable synchronization and visualization of membrane trafficking in living *Drosophila* embryos. These tools allow manipulation of overexpressed or endogenous secretory cargo proteins by reversible ER-retention in intact animals as well as in organs cultured *ex vivo.* The system is broadly applicable to study the spatiotemporal dynamics of secretory trafficking during development *in vivo*. Additionally, we demonstrate that induced ER retention provides a powerful approach to knock-down the function of membrane proteins in a tissue-specific manner.

Results

A two-component system for synchronization of membrane trafficking *in vivo*

To control trafficking of secretory proteins in *Drosophila*, we generated a set of cargo and hook proteins (Fig. 1B) that can be expressed in a tissue-specific manner using the Gal4/UAS system (Brand and Perrimon, 1993). As a model cargo protein we chose the chitin deacetylase Serpentine (Serp), which is secreted apically by tracheal cells into the tube lumen (Luschnig et al., 2006; Wang et al., 2006). We fused the N-terminal signal peptide and chitin-binding domain (CBD) of Serp to Streptavidin-binding peptide (SBP, 38 aa; Keefe et al., 2001) followed by either the EGFP or mRFP coding sequence, yielding Serp(CBD)-SBP-GFP (Serp-SBG) and Serp(CBD)-SBP-mRFP (Serp-SBR), respectively (Fig. 1B). When expressed in tracheal cells under the control of *btl*-Gal4, Serp-SBG and Serp-SBR were secreted into the tracheal lumen, where they accumulated (Fig. 1C,D), resembling endogenous Serp protein (Luschnig et al., 2006; Wang et al., 2006). To retain the fluorescent cargo proteins in the ER, we generated hook constructs comprising either core Streptavidin (SA) or the SA variant Streptactin (ST; Voss and Skerra, 1997) fused to the N-terminal signal peptide of Serp and a C-terminal ER retention signal (KDEL; Fig. 1B). When

expressed in tracheal cells, SA-KDEL and ST-KDEL were distributed in a perinuclear pattern (Fig. 1E,F) and co-localized with anti-KDEL immunostaining (Fig. 1G), indicating localization in the ER.

SBP-tagged proteins can be retained in the ER by Streptavidin hooks

To test whether the streptavidin hooks can retain Serp-SBG in the ER, we co-expressed SA-KDEL and Serp-SBG in tracheal cells. However, expression of a single-copy UAS-SA-KDEL transgene did not modify the distribution of Serp-SBG, which was secreted into the tracheal lumen like in control embryos not expressing SA-KDEL (Fig. 2A,B, Fig. S1). Since SA forms a tetramer with two SBP binding sites (Barrette-Ng et al., 2013), we reasoned that at least a two-fold excess of SA-KDEL will be required for efficient retention of Serp-SBG. Therefore, to increase the levels of SA-KDEL, we used a vector (pUASTΔSV40; Nelson et al., 2018) that yields approximately 5-fold higher expression levels compared to the pUAST vector (Brand and Perrimon, 1993) used for the first generation of SA-KDEL transgenes. Indeed, combining a single copy of UASTΔSV40-SA-KDEL (referred to as UAS-SA-KDEL(strong)) with a single copy of UAS-Serp-SBG led to partial intracellular accumulation of Serp-SBG (Fig. 2C), suggesting that Serp-SBG was partially retained in the ER by SA-KDEL. To further improve the efficiency of retention, we combined multiple copies of UAS-SA-KDEL(strong) transgenes with a single copy of UAS-Serp-SBG (Fig. 2C-E, Fig. S1). Although ER retention was still variable, the ratio of intracellular and luminal Serp-SBG signals ($\text{Serp-SBG}_{\text{intracellular}}$: $\text{Serp-SBG}_{\text{lumen}}$) increased with the dosage of SA-KDEL hooks, and maximal retention (median ratio of 1.2; n=15) was observed in embryos expressing four copies of SA-KDEL (Fig. 2F, Fig. S1).

To ask whether SA-KDEL-mediated ER retention works in different tissues, we generated flies expressing Serp-SBG ubiquitously under the control of the *ubiquitin* promoter (*ubi*-Serp-SBG) and expressed in this background SA-KDEL under the control of tissue-specific Gal4 drivers. In wing imaginal discs of third-instar larvae, Serp-SBG was secreted into the disc lumen (Fig. 2G). Expression of SA-KDEL in in the posterior compartment using *engrailed*-Gal4 (*en*-Gal4) led to intracellular retention of Serp-SBG in the SA-KDEL-expressing cells (Fig. 2H). Similarly, Serp-SBG was retained intracellularly in the larval epidermis, fat body and salivary glands when SA-KDEL was expressed in these tissues (not shown). Thus, SA-KDEL mediates efficient ER retention of an SBP-tagged secreted protein in different tissues and developmental stages.

Injection of biotin triggers ER exit and secretion of SBP-tagged cargo

To test whether SA-KDEL-mediated ER retention is reversible, we injected biotin (1 mM) into the hemocoel of embryos (stage 15) expressing one transgene copy of Serp-SBG and four copies of SA-KDEL (strong) in tracheal cells (Fig. 3). We analyzed the distribution of Serp-SBG in the multicellular dorsal trunk (DT; Fig. 3A,B, Movie S1, Movie S2) and in unicellular dorsal branches (DB; Fig. 3C, Movie S3). Before biotin injection, Serp-SBG was distributed in a perinuclear pattern in tracheal cells. Approximately two minutes after biotin injection, Serp-SBG started to accumulate in discrete intracellular puncta. Six to ten minutes after injection, Serp-SBG signals in the tracheal lumen started to increase rapidly, while intracellular signals concomitantly decreased (Fig. 3A,C,D, Movie S1), indicating that Serp-SBG passed the secretory pathway and started to be secreted as early as six minutes after release from the ER. Luminal Serp-SBG signals were maximal after 30 minutes and then declined gradually, while intracellular signals concurrently leveled off (Fig. 3D), suggesting that the supply of ER-retained Serp-SBG protein was depleted. From approximately 15 minutes after injection, Serp-SBG appeared in small intracellular puncta (0.67 +/- 0.12 µm diameter, mean +/- s.d., n=15 puncta), which moved rapidly (0.43 +/- 0.18 µm/s; mean +/- s.d., n=22 puncta) and co-localized partially with Rab4-mRFP-positive recycling endosomes (Fig. 3B,C', Movie S2, Movie S3). This suggests that secreted Serp-SBG was internalized from the lumen and entered the endocytic pathway, consistent with intense endocytic activity of tracheal cells during luminal clearance (Dong et al., 2013; Tsarouhas et al., 2007).

The kinetics of ER release and luminal secretion of Serp-SBG was dependent on the concentration of injected biotin. 1 mM biotin induced a rapid response, while 10 µM biotin was not sufficient to induce effective ER release (n=3; Fig. S2, Movie S4). A slow and steady increase in luminal Serp-SBG signals upon injection of 10 µM biotin, but no concomitant reduction of intracellular signals, suggests that constant slow leakage of Serp-SBG from the ER is compensated by newly synthesized Serp-SBG protein (Fig. S2).

Taken together, these findings show that biotin injection triggers rapid release of SA-hook-retained proteins from the ER, enabling synchronization of exo- and endocytic protein trafficking in living embryos.

Serp-SBG rapidly passes the secretory apparatus

We used this system to analyze the dynamics of Serp-SBG transport through the early secretory apparatus. Embryonic tracheal cells contain on the order of a dozen dispersed Golgi stacks (Armbruster and Luschnig, 2012; Förster et al., 2010), each of which resides adjacent to a transitional ER (tER; Schweizer et al., 1990) unit, where secretory cargo proteins are collected at clusters of ER exit sites (ERES; Bannykh et al., 1996) before leaving the ER. We labeled ERES using an mCherry-tagged version of the COPII

component Sec24AB (mCherry-Sec24; Fig. 4, Fig. S3), which colocalized with the ERES marker Sec16 (Fig. S3A; Ivan et al., 2008) and localized adjacent to the *cis*-Golgi marker GRASP65-GFP (Fig. S3B; Yang et al., 2021).

To analyze the transit of Serp-SBG through the ER-Golgi interface, we analyzed Serp-SBG signals within spherical volumes, each of which enclosed an mCherry-Sec24-labelled ERES (Fig. 4A,B; Movie S5). Shortly after biotin injection, Serp-SBG rapidly accumulated at mCherry-Sec24-labelled ERES in a synchronous fashion with a peak at seven minutes after injection, and subsequently decreased over 30 minutes (Fig. 4B; n=996 mCherry-Sec24 units in 7 embryos). Afterwards, Serp-SBG levels at ERES leveled off, suggesting that most of the retained Serp-SBG protein has exited the ER. Comparable profiles of Serp-SBG levels were detected in all mCherry-Sec24-labelled tER units analyzed, independent of their position along the apical-basal axis of tracheal cells (Fig. 4C), suggesting that Serp-SBG passes through all ERES/Golgi units in a uniform fashion.

Analyzing the dynamics of Serp-SBG at individual ERES/Golgi units by high-resolution confocal microscopy revealed that Serp-SBG started to accumulate at ERES, as detected by colocalization with mCherry-Sec24, approximately two minutes after biotin injection (Fig. 4D,E; Movie S6). Shortly after, the bulk of Serp-SBG shifted into clusters adjacent to and partially overlapping with the mCherry-Sec24-labelled ERES, before disappearing approximately 20 minutes after biotin injection (Fig. 4D, Movie S6). The area of overlap between mCherry-Sec24 and Serp-SBG signals was maximal between two and six minutes and then dropped to zero approximately 12 minutes after biotin injection (Fig. 4F). These findings suggest that after residing in the tER or at ERES for approximately four minutes, the bulk of Serp-SBG translocates to an adjacent compartment, corresponding to Golgi cisternae (Yang et al., 2021), where the protein spends approximately eight minutes before exiting the Golgi apparatus (Fig. 4E). Thus, RUSH allows analyzing the dynamics of trafficking between different membrane compartments *in vivo*.

Apical secretion in the absence of septate junctions

We applied the RUSH system to understand the effect of mutations on secretion in tracheal tubes. Septate junctions (SJs) are basolateral cell-cell junctions that mediate paracellular barrier function in invertebrate epithelia (Izumi and Furuse, 2014). Embryos lacking SJs show reduced levels of secreted proteins, including Serp, in the tracheal lumen (Fig. S4A,B; Behr et al., 2003; Luschnig et al., 2006; Wang et al., 2006). This could result from leakage of secreted proteins from the lumen in the absence of a functional epithelial barrier (Bätz et al., 2014). Alternatively, SJs could be required for secretory protein trafficking, possibly by acting as an intracellular sorting hub (Wang et al., 2006). To probe the role of SJs in apical

secretion, we analyzed Serp-SBG exocytosis in *pickel* (*pck*, also known as *megatrachea*) mutant embryos, which lack a Claudin-like protein essential for SJ assembly (Behr et al., 2003). Serp-SBG accumulated in the tracheal lumen of pck^{G0012} embryos, albeit at lower levels compared to controls (Fig. S4A,B). Upon ER retention of Serp-SBG by SA-KDEL in tracheal cells, biotin injection triggered release from the ER and secretion of Serp-SGB with similar kinetics in pck^{G0012} embryos as in control embryos (Fig. S4C-E, Movie S7). However, Serp-SBG reached significantly lower levels (49.7% compared to control at t=120 min, p=0.0041, n=5 embryos) in the tracheal lumen of pck^{G0012} embryos (Fig. S4E). Although these findings do not exclude a role of SJs in trafficking of specific proteins, they indicate that SJs are not generally required for apical secretion in tracheal cells, and further suggest that SJs are required for preventing leakage of soluble proteins from the tracheal lumen.

RUSH enables control over trafficking of endogenous proteins

Having shown that secretion of Serp-SBG can be synchronized using SA hooks, we asked whether the system is also applicable to endogenous proteins. To this aim, we took advantage of the Cambridge protein trap insertion (CPTI; Lye et al., 2014) fly strains, in which a given protein is tagged with Venus-YFP and two flanking StrepII tags (StrepII-Venus-YFP-StrepII; SVS) encoded by an artificial exon inserted into the endogenous gene locus (Fig. 5, Fig. S5). We tested transmembrane (Basigin (Bsg; not shown), Echinoid (Ed; not shown), Gliotactin (Gli), Neurexin 4 (Nrx4), Notch (N), Sidekick (Sdk)), Glycosylphosphatidylinositol (GPI)-anchored (Fasciclin 2 (Fas2), Lachesin (Lac)) and secreted (Chitin deacetylase-like 4; Cda4) proteins carrying an SVS tag in their extracellular portion (Fig. S5). To test whether localization of these proteins can be manipulated using ER hooks, we drove expression of ER hooks in epidermal stripes (using *en*-Gal4 or *hh*-Gal4) in heterozygous animals carrying one copy of the SVS-tagged locus (Fig. 5, Fig. S5). To maximize the affinity for StrepII-tagged proteins, we used Streptactin (ST)-KDEL instead of SA-KDEL hook proteins, since the StrepII tag binds with higher affinity to Streptactin (ST-StrepII: $K_d = 10^{-6}$ M; Voss and Skerra, 1997) than to Streptavidin (SA-StrepII: $K_d = 72 \times 10^{-6}$ M; Kim et al., 2010). Expression of two copies of ST-KDEL indeed led to efficient ER retention of SVS-tagged proteins, as shown for Fas2::SVS in the embryonic and larval epidermis, larval imaginal discs, and in adult ovarian follicle cells (Fig. 5A-F). The extent of ER retention varied between different SVS-tagged proteins, from no apparent (Bsg, Ed, Sdk; Fig. S5 and data not shown) or partial (Lac; Fig. S5F) to substantial retention (Cda4, Fas2, Gli, Notch, Nrx4; Fig. S5), suggesting that cargo protein abundance or accessibility of the SVS tag can influence the efficiency of ST-KDEL-induced retention.

In all cases tested, biotin injection triggered rapid release of the retained proteins from the ER. For instance, the SJ protein Nrx4::SVS was retained in the ER in ST-KDEL-expressing epidermal cells, while it was localized at lateral membranes in adjacent control cells (Fig. S5I). Five minutes after biotin injection, Nrx4::SVS accumulated in puncta resembling ERES/Golgi stacks. After fifteen minutes, Nrx4::SVS became detectable at lateral plasma membranes (Fig. S5I, Movie S8), suggesting that the newly released Nrx4::SVS protein was incorporated into SJs.

Real-time analysis of tricellular junction assembly

Building on these findings, we employed RUSH to investigate the assembly of tricellular junctions (TCJs). The transmembrane proteins Anakonda (Aka), Gliotactin (Gli) and M6 accumulate at epithelial cell vertices, where they organize TCJs essential for epithelial barrier function (Schulte et al., 2003; Byri et al., 2015; Wittek et al., 2020), but how TCJ proteins are targeted to vertices is not clear. Analyzing the spatiotemporal dynamics of TCJ assembly has not been possible thus far, because recruitment of TCJ proteins to cell vertices is not apparent under steady-state conditions. We therefore used RUSH to synchronize trafficking of the TCJ protein Gli in the embryonic epidermis. Flies carrying the homozygous viable *Gli*^{CPTI002805} allele (Lye et al., 2014) produce functional Gli::SVS protein that localized to TCJs like wild-type Gli protein (Fig. 6A; Wittek et al., 2020). Expression of two copies of ST-KDEL in epidermal stripes of heterozygous *Gli*^{CPTI002805}/+ embryos led to ER retention of Gli::SVS with only residual signals at TCJs, while Gli::SVS localized to TCJs in adjacent control cells (Fig. 6A,B). Injection of biotin led to a rapid decrease of intracellular Gli::SVS signals and accumulation of Gli::SVS at intracellular puncta resembling ERES-Golgi clusters (Fig. 6B,D, Movie S9). Approximately 8 minutes after biotin injection, Gli::SVS levels began to increase at TCJs (Fig. 6B,D). As there was no apparent intermediate accumulation at bicellular junctions (BCJs), newly synthesized Gli::SVS was either transported directly to TCJs or re-distributed rapidly from BCJs to TCJs (Fig. 6B,D). Interestingly, the newly released Gli::SVS protein was not incorporated along the entire length of TCJs, but first accumulated at the apical side of pre-existing TCJs (Fig. 6C), suggesting that growing TCJs are extended by addition of new material to the apical side of the junctional complex, resembling growing SJs (Wittek et al., 2020; Babatz et al., 2018). These findings demonstrate how synchronization of membrane trafficking can be employed to gain insights into the spatiotemporal dynamics of junctional complex assembly in developing tissues *in vivo*.

Synchronization of membrane trafficking in organs cultured *ex vivo*

We next asked whether RUSH also allows controlling secretory trafficking in cultured organs *ex vivo*. To this aim, we cultured ovarian follicles of adult females expressing Fas2 tagged at its endogenous locus with an SVS-encoding exon (Fas2::SVS, CPTI 000483; Lye et al., 2014). Fas2 encodes transmembrane and GPI-anchored isoforms (Neuert et al., 2020), all of which carry the SVS tag in the Fas2 extracellular domain. Fas2::SVS localized along lateral membranes of follicle cells in pre-vitellogenic egg chambers (Fig. 5E). Expression of ST-KDEL in the follicle epithelium of heterozygous *Fas2::SVS*/+ females led to retention of Fas2::SVS in the perinuclear ER of follicle cells (Fig. 5F). Addition of biotin (1 mM final concentration) to the culture medium triggered release of Fas2::SVS from the ER after approximately five minutes (n=8; Movie S10). At the same time, Fas2::SVS began to accumulate in large vesicular structures, and became detectable at lateral cell membranes 20 minutes after biotin addition (Fig. 5G).

Taken together, these findings show that endogenous transmembrane, GPI-anchored, and secreted proteins can be trapped in the ER using streptavidin hooks and can be released upon biotin addition in embryos as well as in organs cultured *ex vivo*.

ER retention enables tissue-specific interference with protein function

Finally, we asked whether hook-induced ER retention could be employed to interfere with protein function. To this aim, we analyzed the effect of ER retention of the Notch (N) receptor on cell fate specification. In the embryonic tracheal system, the N ligand Delta (Dl) is expressed at elevated levels in tracheal fusion cells (FCs) at branch tips and activates N signaling in adjacent stalk cells to prevent these cells from adopting tip cell fate (Fig. 7A). Accordingly, *N* mutations cause excessive FC specification (Ikeya and Hayashi, 1999; Llimargas, 1999; Steneberg et al., 1999). To test whether ST-KDEL-induced ER retention of N protein in tracheal cells can reproduce the tracheal phenotype of *N* mutations, we used the $N^{SVS\text{-}CPTI002347}$ protein trap allele (referred to as *N::SVS*), which produces a N::SVS protein with an SVS tag in the N ectodomain (Lye et al., 2014). N::SVS protein was weakly detectable in embryonic tracheal (Fig. 7B) and larval wing imaginal disc cells (Fig. 7D). Homozygous (female) and hemizygous (male) *N::SVS* flies were phenotypically normal and fertile, indicating that N::SVS protein is functional. The majority of embryos carrying *N::SVS* showed normal tracheal cell specification with a pair of FCs (discernible by expression of the transcription factor Dysfusion (Dysf)) at each tracheal metamere boundary (Fig. 7B), while supernumerary FCs were found in 12% (n=17) of *N::SVS*/+ heterozygous and in 43% (n=14) of *N::SVS/Y* hemizygous embryos (at least one extra FC per embryo; Fig. S6A,B,G). Expression of two copies of ST-KDEL in tracheal cells of *N::SVS* embryos led to intracellular accumulation of N::SVS protein (Fig. 7C) and to excessive specification of FCs in 31%

(n=13) of *N::SVS/+* heterozygous and in 76% (n=21) of *N::SVS/Y* hemizygous embryos (Fig. S6C,D,G). Increasing the dosage of *btl*-Gal4 from one to two copies led to fully penetrant (100%; n=11) ectopic FC specification in *N::SVS/Y* hemizygous embryos (Fig. S7F,G), indicating that hook-induced ER retention of N protein effectively blocks N signaling. Moreover, expression of ST-KDEL under the control of *en*-Gal4 led to ER retention of N::SVS protein in the posterior compartment of wing imaginal discs in third-instar larvae (Fig. 7D). Adult flies showed characteristic wing margin defects and thickened wing veins, resembling the wing defects of N^1 mutants, but restricted to the posterior wing compartment (Fig. 7E-G). Together, these findings demonstrate that hook-induced ER retention can be used to deplete the functional pool of a membrane protein by interfering with its secretion in a tissue-specific manner.

Discussion

We present a system that enables visualizing the dynamics of membrane trafficking through reversible retention of proteins in the secretory apparatus in a multicellular organism. We show that secreted, transmembrane, and GPI-linked proteins can be efficiently retained in the ER by streptavidin hook proteins in *Drosophila* embryos, larvae and adults. Hook-mediated ER retention is rapidly reversed upon addition of biotin, allowing to synchronize intracellular trafficking and to release fluorescent-marked cargo proteins with high temporal precision in a burst of secretion. The system enables control of exogenous and endogenous proteins, is readily combined with available endogenously tagged protein trap alleles, and is applicable to various tissues in intact animals, as well to organs cultured *ex vivo*. We demonstrate the utility of this approach for analyzing the kinetics of protein secretion and the spatiotemporal dynamics of tricellular junction assembly in embryonic epithelia. Finally, we show that hook-induced ER retention can be employed to deplete the functional pool of proteins, allowing to generate tissue-specific loss-of-function conditions.

RUSH represents a versatile two-component system based on short peptide tags (SBP or StrepII) that can be fused to any protein of interest and enable control at physiological temperature by biotin, an endogenous vitamin (Boncompain et al., 2012). Injection of biotin at concentrations presumably far exceeding physiological levels did not cause apparent toxicity in *Drosophila* embryos. However, the presence of endogenous biotin is expected to reduce the efficacy of hook-induced cargo retention by occupying SBP binding sites on streptavidin. We show that this problem can be overcome by increasing the dosage of streptavidin-KDEL hook proteins, and we generated fly stocks carrying multiple copies of streptavidin transgenes, enabling straightforward use of these tools in genetic crosses.

Considering that streptavidin-KDEL hooks mediate efficient retention of secreted and transmembrane proteins in the ER, we also tested whether SVS-tagged cytoplasmic proteins (α-Catenin, β-Catenin, Amphiphysin) can be relocalized by membrane-tethered (ST-CAAX) or nuclear-localized (ST-NLS) Streptactin-hook constructs (not shown). However, in no case did we observe hook-induced relocalization of cytoplasmic proteins, possibly because free biotin in the cytosol (where it may be present at higher concentrations than in the ER lumen) might saturate Streptavidin hooks and thereby prevent binding of cargo. Conversely, high-level expression of SA-KDEL or ST-KDEL led to developmental delays or reduced viability. This was not accompanied by ER stress, as expression of the ER stress reporter XBP-1-GFP (Ryoo et al., 2007) was not induced by hook-mediated ER retention of RUSH cargos (data not shown), suggesting that adverse effects of high-level streptavidin expression are not caused by elevated secretory load, but are rather due to depletion of biotin, an essential vitamin, by streptavidin. However, these potential problems can be avoided by tuning the levels or timing of Streptavidin expression, e.g. using temperature-sensitive Gal80 to conditionally control Gal4 activity (McGuire et al., 2004).

The use of RUSH revealed rapid ER exit and passage of the Golgi apparatus by secretory proteins in epithelia *in vivo*. While mammalian cells typically contain a single pile of interconnected Golgi stacks with tubular ERES extending between ER and Golgi (Weigel et al., 2021), *Drosophila* cells contain several dispersed Golgi mini-stacks (Kondylis and Rabouille, 2009) adjacent to C- or ring-shaped ERES (Reynolds et al., 2019; Yang et al., 2021). Despite these differences, ER-Golgi trafficking in *Drosophila* tracheal cells occurred on similar time scales (2 to 3 min for Serp-SBG) as described for various GPI-linked and transmembrane RUSH cargos in mammalian cells (Weigel et al., 2021). Overexpressed Serp-SBG was released from the ER with similar kinetics as endogenous proteins (Fas2:SVS, Gli::SVS; Nrx4::SVS), suggesting that rapid ER-Golgi traffic is not due to overexpression of a cargo protein. However, unlike in mammalian cells, where trafficking of TNF-alpha led to a two-fold size increase of ERES (Weigel et al., 2021), we did not detect obvious changes in the size of mCherry-Sec24-labelled ERES upon ER-release of cargo in tracheal cells. Previous work indicated that subsets of Golgi units in *Drosophila* epithelial cells contain distinct sets of glycosylation enzymes, suggesting possible functional differences between Golgi units (Yano et al., 2005). For the secretory proteins tested here, we did not detect evident differences in the rate of cargo passage between different ERES, all of which appeared to be traversed in an approximately uniform fashion. This suggests that functional differences between individual ER-Golgi units are not reflected by the dynamics of cargo passage through these units.

Our real-time analysis of tricellular junction assembly demonstrates the potential of the RUSH assay for elucidating the intracellular routes of proteins and the kinetics of their assembly into complex structures at the tissue level in living organisms. Importantly, the ability to synchronize and follow the dynamics of these processes in real time reveals insights that are not apparent at steady state or by endpoint analysis of mutant phenotypes, as we demonstrated by analyzing protein secretion in the absence of functional septate junctions. In addition to analyzing secretory trafficking in intact living animals, we demonstrate that hook-induced protein re-localization can be used to interfere with protein function. Manipulating proteins rather than gene expression is required in situations where perdurance of proteins due to slow turnover upon genetic knockout or RNAi-mediated knock-down precludes loss-of-function phenotypes. While nanobody-based approaches allow to interfere with proteins by re-localizing (Harmansa et al., 2017), trapping (Matsuda et al., 2021) or degrading them (Caussinus et al., 2012), reversible retention by streptavidin hooks offers the additional potential to acutely restore protein localization and function upon addition of biotin. This will enable powerful functional experiments with precise temporal control, for instance allowing to release a signaling molecule from a defined source at a defined time and to determine the spatiotemporal dynamics of dispersal of the signaling molecule in the tissue and its effects across a field of cells.

While RUSH provides temporal control over protein localization, the system can be combined with orthogonal opto-chemical tools (e.g., photoactivatable “caged” biotin; Terai et al., 2011) or with photoactivatable or photoconvertible proteins to enable precise spatial and temporal manipulation of cellular processes. We anticipate that the application and further development of the tools presented here will reveal new insights into the dynamics and functions of secretory trafficking in various model organisms.

Materials and methods

Drosophila strains and genetics

Unless noted otherwise, *Drosophila* stocks are described in FlyBase. Cambridge protein trap insertion (CPTI) lines (Lye et al., 2014) were obtained from the DGRC (Kyoto, Japan) stock center for Basigin (Bsg; CPTI 100050), Chitin deacetylase-like 4 (Cda4; CPTI 002501), Echinoid (Ed; CPTI 000616), Fasciclin 2 (Fas2; CPTI 000483), Gliotactin (Gli; CPTI 002805), Lachesin (Lac; CPTI 002601), Neurexin 4 (Nrx4; CPTI 001977), Notch (N; CPTI 002347) and Sidekick (Sdk; CPTI001692). Other fly stocks were *pck*^{G0012} (Behr et al., 2003), UAS-mCherry-Sec24 (this work), UAS-Rab4-mRFP (Bloomington 8505), UAS-mCherry-NLS, UAS-CyPET-nls (Caussinus et al., 2008), UAS-palm-mKate2 (Caviglia et al., 2016), UAS-

palm-mNeonGreen (Sauerwald et al., 2017), UAS-SerpCBD-GFP (Luschnig et al., 2006), *ubi*-Dlg1::mTagRFP (Pinheiro et al., 2017), *btl*-GAL4, *en*-GAL4, *GR1*-Gal4, *hh*-GAL4, *CyO Dfd-GMR-nvYFP, TM6b Dfd-GMR-nvYFP* (Le et al., 2006). The *TM3 Ser Dfd-GMR-nvYFP* balancer chromosome was generated by transposase-mediated mobilization of the *P[Dfd-GMR-nvYFP]* P-element from the *FM7i Dfd-GMR-nvYFP* chromosome (Le et al., 2006) onto a *TM3 Ser* chromosome.

Transgenic constructs

The following cargo and hook constructs were generated in this work: Serp-SBG (pUAST-SerpCBD-SBP-GFP, pWRpUbiqPE-SerpCBD-SBP-GFP), Serp-SBR (pUAST-Serp(CBD)-SBP-mRFP), Streptavidin-KDEL (pUAST-SA-KDEL, pUAST∆SV40-SA-KDEL), Streptactin-KDEL (pUAST∆SV40-ST-KDEL).

Serp(CBD)-SBP-GFP (Serp-SBG) was generated as follows: A DNA fragment containing the N-terminal part of the Serp coding sequence including the signal peptide (aa1-25; Luschnig et al., 2006) and chitin-binding domain (CBD) and one copy of Streptavidin-binding peptide (SBP; 38 aa; Keefe et al., 2001) was synthesized and cloned into pUC57-KanR (GenScript Inc.). The insert was subcloned as an EcoRI-NotI fragment into pUASTattB-EGFP to introduce a C-terminal EGFP tag. The construct was integrated into the attP-3B/22A3 landing site using PhiC31-mediated site-specific integration (Bischof et al., 2007). For ubiquitous expression under the control of the *ubiquitin* promoter, the Serp-SBG coding sequence was inserted into pWRpUbiqPE and transformed into *y w* flies via P-element mediated transgenesis.

Serp(CBD)-SBP-mRFP (Serp-SBR) was generated as follows: A DNA fragment comprising the N-terminal part of Serp, an SBP tag and the mRFP coding sequence was synthesized and cloned into pUC57-KanR (GenScript Inc.) and subcloned as an EcoRI-XBaI fragment into pUASTattB (Bischof et al., 2007). The construct was integrated into the attP40/25C6 landing site.

Streptavidin-KDEL (SA-KDEL) was generated by fusing the core SA coding sequence (UniProt P22629; aa 36-163) to the N-terminal signal peptide of Serp (aa 1-25) and to a C-terminal four-amino-acid ER retention signal (KDEL). The protein sequence was reverse-translated using the *Drosophila melanogaster* codon usage distribution, synthesized, and cloned into pUC57-KanR (GenScript, Inc.), and subcloned as an EcoRI-XbaI fragment into pUASTattB (Bischof et al., 2007) and pUAST∆SV40attB, respectively. pUAST∆SV40attB is a pUASTattB derivative lacking the SV40 3'-UTR that targets transcripts for nonsense-mediated mRNA decay. Deletion of the intron-containing 3'-UTR yields stabilized transcripts and approximately 5-fold higher expression levels compared to pUAST transgenes (Nelson

et al., 2018). The pUAST∆SV40attB-SA-KDEL construct was integrated into attP40/25C6, attP/51C1, attP-3B/62E1 and attP/86E18 landing sites. The pUAST-SA-KDEL construct was integrated into the attP2/68A4 landing site.

Streptactin-KDEL (ST-KDEL) was generated by fusing the ST coding sequence (Voss and Skerra, 1997) to the N-terminal signal peptide of Serp (aa 1-25) and a C-terminal ER retention signal (KDEL). This fragment was synthesized, inserted in pUC57-KanR (GenScript, Inc.), and subcloned as an EcoRI-KpnI fragment in pUAST∆SV40attB. The construct was integrated into the attP-3B/62E1 and attP/86E18 landing sites.

To increase the copy number of SA-KDEL or ST-KDEL transgenes, two insertions on the second chromosome (attP40/25C6, attP/51C1) and two insertions on the third chromosome (attP-3B/62E1, attP/86E18), respectively, were recombined. A strain carrying four copies of UAS-SA-KDEL was generated by combining two insertions on the second chromosome (attP40/25C6, attP/51C1) with two insertions on the third chromosome (attP-3B/62E, attP/86E18).

mCherry-Sec24 was generated by amplifying the *Sec24AB* coding region (including introns) from genomic DNA of Oregon R flies using oligonucleotides BamHI-sec24-F (5'-ATATGGATCCATGTCGACTTACAATCCGAAC) and sec24-XbaI-R (5'-TATATCTAGATCGCTTCGTGCTTCTAGTCA). The PCR product was cut with BamHI and XbaI and the resulting fragment was inserted into pUASTattB-mCherry-mcs (BglII-XbaI) to fuse mCherry to the N-terminus of Sec24. The pUASTattB-mCherry-Sec24 construct was integrated into the attP/ZH-86Fa landing site. After establishing a homozygous viable transformant line, the w^+ and *3xP3-RFP* markers of the attP/ZH-86Fa landing site were removed using Cre recombinase.

Antibodies and immunostainings

Embryos were fixed in 4% formaldehyde in PBS/heptane for 20 minutes and devitellinized by shaking in methanol/heptane. The following antibodies were used: chicken anti-GFP (1:500; Abcam 13970), mouse anti-GFP mAB 12A6 (1:300; DSHB), mouse anti-mCherry (1:200; Biorbyt orb66657), chicken anti-mCherry (1:1000; Novus NBP2-25158SS), mouse anti-Streptavidin (1:500; Abcam S10D4, ab10020), rabbit anti-Streptavidin (1:200; Abcam ab6676), rabbit anti-Serp (1:300; Luschnig et al., 2006) mouse anti-KDEL (1:100; Abcam 10C3), rabbit anti-Dysfusion (1:500; Jiang and Crews, 2003), rabbit-anti-Sec16 (1:1000; Ivan et al., 2008), mouse anti-Sxl M18-c (1:500; DSHB). Goat secondary antibodies were conjugated with Alexa 488, Alexa 568, Alexa 647 (Molecular Probes), or Cy5 (Jackson ImmunoResearch). Chitin was detected using AlexaFluor-labeled chitin-binding domain from *Bacillus circulans* chitinase A1 as described in (Caviglia and Luschnig, 2013).

Microscopy and microinjections

For live imaging, embryos (12-15 h AEL) were dechorionated and spread on apple juice agar plates. Embryos were visually selected for ER retention of GFP-tagged cargo proteins and staged according to tracheal and midgut morphology using a Leica M165 FC fluorescence stereomicroscope. Selected embryos were lined up on apple juice agar blocks, transferred to glue-coated coverslips, and covered with Voltalef 10S halocarbon oil before injection with D-biotin (B4501; Sigma-Aldrich) at the indicated concentration (unless indicated otherwise, 1 mM in water). Biotin injections were performed using either a Transjector 5246 microinjector (Eppendorf) with Femtotips II at a transmitted light microscope (Standard 25 ICS, Zeiss) or using a FemtoJet microinjector (Eppendorf) mounted on an inverted Leica SP8 confocal microscope. Embryos were imaged using 40x/1.3 NA and 60x/1.35 NA objectives on an Olympus FV1000 inverted confocal microscope or using 40x/1.3 NA and 60x/1.4 NA objectives on a Leica SP8 inverted confocal microscope.

For high-resolution imaging of ER exit sites, embryos were prepared as described above and imaged using a 63x/1.4 NA objective on a Leica SP8 confocal microscope. Images were deconvolved with Huygens Professional version 16.10 (Scientific Volume Imaging, The Netherlands, http://svi.nl) using the CMLE algorithm with SNR:15 and 40 iterations.

Culture and imaging of ovarian follicles

Adult females expressing Fas2::SVS (CPTI000483) and two copies of ST-KDEL under the control of the follicle-cell specific *GR1*-Gal4 driver were fed on yeast at 27°C for two days after eclosion. Ovaries were dissected in M3 insect medium (Sigma) containing 0.05% $KHCO_3$ and 1x penicillin/streptomycin (from 100x stock; Thermo Fisher). To minimize the biotin content of the medium, yeast extract and Bacto Peptone were not added. Dissected follicles were transferred to 8-well glass-bottom chambers (VWR 734-2061) containing 200 µl medium per well. Chambers were coated with poly-D-Lysine (0.1 mg/ml in water, pH 8.5; Sigma) for 1 h at 37°C before use to immobilize follicles on the glass surface. To induce release of ER-retained proteins, 200 µl of biotin (3 mM in M3 medium) were added to the medium (1.5 mM final biotin concentration) during imaging.

Image analysis

Images were processed using Fiji/ImageJ (v1.42), Imaris (v7.7.0; Bitplane), OMERO (5.4.10) and Adobe Photoshop. Serp-SBG signals in tracheal cells and lumen, respectively, were measured in manually selected regions of interest (ROI) on average projections of confocal sections acquired in tracheal DT metamere 7. Background intensity was measured in the hemocoel outside the trachea and subtracted from intracellular and luminal signals. Serp-

SBG-containing vesicles (endosomes) were segmented by applying a median filter (radius 2.0) and a manual threshold. Vesicle diameter (Feret distance) was measured using the Analyze Particles plugin in Fiji.

For quantifying Gli::SVS signals, mean gray values at TCJs and inside cells, respectively, were measured in manually drawn ROIs for each time point on average projections of the three most apical slices showing junctional signal in a z-stack. For each time point, the mean intensity for TCJs and intracellular signals, respectively, was calculated. The values were then normalized to the mean of the first three time points per group (TCJ vs. intracellular signals.

For analyzing the dynamics of Serp-SBG at ER exit sites, mCherry-Sec24-labeled ERES were segmented using the Imaris 3D Spot function. Serp-SBG signals within spherical mCherry-Sec24-containing volumes were measured in Imaris. To quantify the area of intersection between mCherry-Sec24 and Serp-SBG signals at ERES, the signals were segmented using Default (for mCherry-Sec24) and Yen Fiji (for Serp-SBG) automatic threshold methods, respectively. The area of intersection was measured using Fiji.

Statistics

Statistical analyses were performed in Microsoft Excel 2010, OriginLab 8.5, or R (3.5.1) using RStudio Interface (1.3.1093). Sample size (n) was not predetermined using statistical methods, but was assessed empirically by taking into account the variability of a given effect as determined by the standard deviation. Experiments were considered independent if the specimens analyzed were derived from different parental crosses. Investigators were not blinded to allocation during experiments. The data was tested for normality using the Shapiro-Wilk test. Student's t-test was used for normally distributed data. When the data was not normally distributed, the Wilcoxon rank-sum test (R standard package) was used. P values were corrected for multiple testing using the Bonferroni-Holm method (Holm, 1979). Sample size (n) is indicated in the graphs or figure legends.

Author contributions

Conceptualization, J.G., C.C., S.L.; Methodology, all authors; Investigation, J.G., C.C., M.H., J.I.S., T.J., W.B.; Formal Analysis, J.G., C.C., M.H.; Visualization, J.G., C.C., M.H., J.I.S., T.J., W.B.; Reagents and tools, J.G., C.C., M.H., T.J., W.B., D.F., S.L.; Writing – Original Draft, J.G., C.C.; Writing – Review and Editing, C.C., S.L.; Funding Acquisition, S.L; Supervision, S.L.

Acknowledgements

We thank Franck Perez for advice and discussions, Veit Riechmann for comments on the manuscript, and Raphael Schleutker for help with data analysis and statistics.

Funding

J.G. was supported by a Forschungskredit fellowship of the University of Zürich. Work in SL's laboratory was supported by the Deutsche Forschungsgemeinschaft (SFB 1348 "Dynamic Cellular Interfaces"; SFB 1009 "Breaking Barriers"), the Swiss National Science Foundation (SNF 31003A_141093_1), the "Cells-in-Motion" Cluster of Excellence (EXC 1003-CiM) at the University of Münster, and the University of Münster.

Competing interests

The authors declare that they have no conflict of interest.

References

Armbruster, K., and Luschnig, S. (2012). The Drosophila Sec7 domain guanine nucleotide exchange factor protein Gartenzwerg localizes at the cis-Golgi and is essential for epithelial tube expansion. J. Cell Sci. *125*, 1318–1328.

Babatz, F., Naffin, E., and Klämbt, C. (2018). The Drosophila Blood-Brain Barrier Adapts to Cell Growth by Unfolding of Pre-existing Septate Junctions. Dev. Cell *47*, 697-710.e3.

Bannykh, S.I., Rowe, T., and Balch, W.E. (1996). The organization of endoplasmic reticulum export complexes. J. Cell Biol. *135*, 19–35.

Barrette-Ng, I.H., Wu, S.C., Tjia, W.M., Wong, S.L., and Ng, K.K. (2013). The structure of the SBP-Tag-streptavidin complex reveals a novel helical scaffold bridging binding pockets on separate subunits. Acta Crystallogr Biol Crystallogr *69*, 879–887.

Bätz, T., Förster, D., and Luschnig, S. (2014). The transmembrane protein Macroglobulin complement-related is essential for septate junction formation and epithelial barrier function in Drosophila. Development *141*, 899–908.

Behr, M., Riedel, D., and Schuh, R. (2003). The claudin-like megatrachea is essential in septate junctions for the epithelial barrier function in Drosophila. Dev Cell *5*, 611–620.

Bischof, J., Maeda, R.K., Hediger, M., Karch, F., and Basler, K. (2007). An optimized transgenesis system for Drosophila using germ-line-specific phiC31 integrases. Proc Natl Acad Sci U A *104*, 3312–3317.

Boncompain, G., Divoux, S., Gareil, N., de Forges, H., Lescure, A., Latreche, L., Mercanti, V., Jollivet, F., Raposo, G., and Perez, F. (2012). Synchronization of secretory protein traffic in populations of cells. Nat Methods *9*, 493–498.

Brand, A.H., and Perrimon, N. (1993). Targeted gene expression as a means of altering cell fates and generating dominant phenotypes. Development *118*, 401–415.

Byri, S., Misra, T., Syed, Z.A., Bätz, T., Shah, J., Boril, L., Glashauser, J., Aegerter-Wilmsen, T., Matzat, T., Moussian, B., et al. (2015). The Triple-Repeat Protein Anakonda Controls Epithelial Tricellular Junction Formation in Drosophila. Dev Cell *33*, 535–548.

Caussinus, E., Colombelli, J., and Affolter, M. (2008). Tip-Cell Migration Controls Stalk-Cell Intercalation during Drosophila Tracheal Tube Elongation. Curr. Biol. *18*, 1727–1734.

Caussinus, E., Kanca, O., and Affolter, M. (2012). Fluorescent fusion protein knockout mediated by anti-GFP nanobody. Nat Struct Mol Biol *19*, 117–121.

Caviglia, S., and Luschnig, S. (2013). The ETS domain transcriptional repressor Anterior open inhibits MAP kinase and Wingless signaling to couple tracheal cell fate with branch identity. Development *140*, 1240–1249.

Caviglia, S., Brankatschk, M., Fischer, E.J., Eaton, S., and Luschnig, S. (2016). Staccato/Unc-13-4 controls secretory lysosome-mediated lumen fusion during epithelial tube anastomosis. Nat Cell Biol *18*, 727–739.

Chen, D., Gibson, E.S., and Kennedy, M.J. (2013). A light-triggered protein secretion system. J. Cell Biol. *201*, 631–640.

Dong, B., Kakihara, K., Otani, T., Wada, H., and Hayashi, S. (2013). Rab9 and retromer regulate retrograde trafficking of luminal protein required for epithelial tube length control. Nat. Commun. *4*, 1358.

Förster, D., Armbruster, K., and Luschnig, S. (2010). Sec24-dependent secretion drives cell-autonomous expansion of tracheal tubes in Drosophila. Curr Biol *20*, 62–68.

Fourriere, L., Divoux, S., Roceri, M., Perez, F., and Boncompain, G. (2016). Microtubule-independent secretion requires functional maturation of Golgi elements. J. Cell Sci. *129*, 3238–3250.

Griffiths, G., Pfeiffer, S., Simons, K., and Matlin, K. (1985). Exit of newly synthesized membrane proteins from the trans cisterna of the Golgi complex to the plasma membrane. J. Cell Biol. *101*, 949–964.

Harmansa, S., Alborelli, I., Bieli, D., Caussinus, E., and Affolter, M. (2017). A nanobody-based toolset to investigate the role of protein localization and dispersal in Drosophila. ELife *6*, e22549.

Holm, S. (1979). A Simple Sequentially Rejective Multiple Test Procedure. Scand. J. Stat. *6*, 65–70.

Ikeya, T., and Hayashi, S. (1999). Interplay of Notch and FGF signaling restricts cell fate and MAPK activation in the Drosophila trachea. Development *126*, 4455–4463.

Ivan, V., de Voer, G., Xanthakis, D., Spoorendonk, K.M., Kondylis, V., and Rabouille, C. (2008). Drosophila Sec16 Mediates the Biogenesis of tER Sites Upstream of Sar1 through an Arginine-Rich Motif. Mol. Biol. Cell *19*, 4352–4365.

Izumi, Y., and Furuse, M. (2014). Molecular organization and function of invertebrate occluding junctions. Semin. Cell Dev. Biol. *36*, 186–193.

Jiang, L., and Crews, S.T. (2003). The Drosophila dysfusion Basic Helix-Loop-Helix (bHLH)-PAS Gene Controls Tracheal Fusion and Levels of the Trachealess bHLH-PAS Protein. Mol. Cell. Biol. *23*, 5625–5637.

Keefe, A.D., Wilson, D.S., Seelig, B., and Szostak, J.W. (2001). One-step purification of recombinant proteins using a nanomolar-affinity streptavidin-binding peptide, the SBP-Tag. Protein Expr Purif *23*, 440–446.

Kim, J.H., Chang, T.M., Graham, A.N., Andy Choo, K.H., Kalitsis, P., and Hudson, D.F. (2010). Streptavidin-Binding Peptide (SBP)-tagged SMC2 allows single-step affinity fluorescence, blotting or purification of the condensin complex. BMC Biochem. *11*, 50.

Kondylis, V., and Rabouille, C. (2009). The Golgi apparatus: lessons from Drosophila. FEBS Lett *583*, 3827–3838.

Kreis, T.E., and Lodish, H.F. (1986). Oligomerization is essential for transport of vesicular stomatitis viral glycoprotein to the cell surface. Cell *46*, 929–937.

Lafay, F. (1974). Envelope proteins of vesicular stomatitis virus: effect of temperature-sensitive mutations in complementation groups III and V. J Virol *14*, 1220–1228.

Le, T., Liang, Z., Patel, H., Yu, M.H., Sivasubramaniam, G., Slovitt, M., Tanentzapf, G., Mohanty, N., Paul, S.M., Wu, V.M., et al. (2006). A new family of Drosophila balancer chromosomes with a w- dfd-GMR yellow fluorescent protein marker. Genetics *174*, 2255–2257.

Lippincott-Schwartz, J., Yuan, L.C., Bonifacino, J.S., and Klausner, R.D. (1989). Rapid redistribution of Golgi proteins into the ER in cells treated with brefeldin A: evidence for membrane cycling from Golgi to ER. Cell *56*, 801–813.

Llimargas, M. (1999). The Notch pathway helps to pattern the tips of the Drosophila tracheal branches by selecting cell fates. Development *126*, 2355–2364.

Luschnig, S., Bätz, T., Armbruster, K., and Krasnow, M.A. (2006). serpentine and vermiform encode matrix proteins with chitin binding and deacetylation domains that limit tracheal tube length in Drosophila. Curr Biol *16*, 186–194.

Lye, C.M., Naylor, H.W., and Sanson, B. (2014). Subcellular localisations of the CPTI collection of YFP-tagged proteins in Drosophila embryos. Development *141*, 4006–4017.

Matsuda, S., Schaefer, J.V., Mii, Y., Hori, Y., Bieli, D., Taira, M., Plückthun, A., and Affolter, M. (2021). Asymmetric requirement of Dpp/BMP morphogen dispersal in the Drosophila wing disc. Nat. Commun. *12*, 6435.

McGuire, S.E., Mao, Z., and Davis, R.L. (2004). Spatiotemporal gene expression targeting with the TARGET and gene-switch systems in Drosophila. Sci. STKE Signal Transduct. Knowl. Environ. *2004*, pl6.

Meinken, J., Walker, G., Cooper, C.R., and Min, X.J. (2015). MetazSecKB: the human and animal secretome and subcellular proteome knowledgebase. Database *2015*, bav077.

Nelson, J.O., Förster, D., Frizzell, K.A., Luschnig, S., and Metzstein, M.M. (2018). Multiple Nonsense-Mediated mRNA Processes Require Smg5 in Drosophila. Genetics *209*, 1073–1084.

Neuert, H., Deing, P., Krukkert, K., Naffin, E., Steffes, G., Risse, B., Silies, M., and Klämbt, C. (2020). The *Drosophila* NCAM homolog Fas2 signals independently of adhesion. Development *147*, dev181479.

Pei, J., Kinch, L.N., and Grishin, N.V. (2018). FlyXCDB—A Resource for Drosophila Cell Surface and Secreted Proteins and Their Extracellular Domains. J. Mol. Biol. *430*, 3353–3411.

Pinheiro, D., Hannezo, E., Herszterg, S., Bosveld, F., Gaugue, I., Balakireva, M., Wang, Z., Cristo, I., Rigaud, S.U., Markova, O., et al. (2017). Transmission of cytokinesis forces via E-cadherin dilution and actomyosin flows. Nature *545*, 103–107.

Reynolds, H.M., Zhang, L., Tran, D.T., and Ten Hagen, K.G. (2019). Tango1 coordinates the formation of endoplasmic reticulum/Golgi docking sites to mediate secretory granule formation. J. Biol. Chem. *294*, 19498–19510.

Ryoo, H.D., Domingos, P.M., Kang, M.-J., and Steller, H. (2007). Unfolded protein response in a Drosophila model for retinal degeneration. EMBO J. *26*, 242–252.

Sauerwald, J., Soneson, C., Robinson, M.D., and Luschnig, S. (2017). Faithful mRNA splicing depends on the Prp19 complex subunit faint sausage and is required for tracheal branching morphogenesis in Drosophila. Development *144*, 657–663.

Schotman, H., and Rabouille, C. (2009). The Exocytic Pathway and Development. In Trafficking Inside Cells, (New York, NY: Springer New York), pp. 419–438.

Schulte, J., Tepass, U., and Auld, V.J. (2003). Gliotactin, a novel marker of tricellular junctions, is necessary for septate junction development in Drosophila. J Cell Biol *161*, 991–1000.

Schweizer, A., Fransen, J.A., Matter, K., Kreis, T.E., Ginsel, L., and Hauri, H.P. (1990). Identification of an intermediate compartment involved in protein transport from endoplasmic reticulum to Golgi apparatus. Eur. J. Cell Biol. *53*, 185–196.

Shomron, O., Nevo-Yassaf, I., Aviad, T., Yaffe, Y., Zahavi, E.E., Dukhovny, A., Perlson, E., Brodsky, I., Yeheskel, A., Pasmanik-Chor, M., et al. (2021). COPII collar defines the boundary between ER and ER exit site and does not coat cargo containers. J. Cell Biol. *220*, e201907224.

Stalder, D., and Gershlick, D.C. (2020). Direct trafficking pathways from the Golgi apparatus to the plasma membrane. Semin. Cell Dev. Biol. *107*, 112–125.

Steneberg, P., Hemphälä, J., and Samakovlis, C. (1999). Dpp and Notch specify the fusion cell fate in the dorsal branches of the Drosophila trachea. Mech. Dev. *87*, 153–163.

Terai, T., Maki, E., Sugiyama, S., Takahashi, Y., Matsumura, H., Mori, Y., and Nagano, T. (2011). Rational development of caged-biotin protein-labeling agents and some applications in live cells. Chem Biol *18*, 1261–1272.

Tsarouhas, V., Senti, K.A., Jayaram, S.A., Tiklová, K., Hemphälä, J., Adler, J., and Samakovlis, C. (2007). Sequential pulses of apical epithelial secretion and endocytosis drive airway maturation in Drosophila. Dev Cell *13*, 214–225.

Voss, S., and Skerra, A. (1997). Mutagenesis of a flexible loop in streptavidin leads to higher affinity for the Strep-tag II peptide and improved performance in recombinant protein purification. Protein Eng *10*, 975–982.

Wang, S., Jayaram, S.A., Hemphälä, J., Senti, K.A., Tsarouhas, V., Jin, H., and Samakovlis, C. (2006). Septate-junction-dependent luminal deposition of chitin deacetylases restricts tube elongation in the Drosophila trachea. Curr Biol *16*, 180–185.

Weigel, A.V., Chang, C.-L., Shtengel, G., Xu, C.S., Hoffman, D.P., Freeman, M., Iyer, N., Aaron, J., Khuon, S., Bogovic, J., et al. (2021). ER-to-Golgi protein delivery through an interwoven, tubular

network extending from ER. Cell *184*, 2412-2429.e16.

Westrate, L.M., Hoyer, M.J., Nash, M.J., and Voeltz, G.K. (2020). Vesicular and uncoated Rab1-dependent cargo carriers facilitate ER to Golgi transport. J. Cell Sci. *133*, jcs239814.

Wittek, A., Hollmann, M., Schleutker, R., and Luschnig, S. (2020). The Transmembrane Proteins M6 and Anakonda Cooperate to Initiate Tricellular Junction Assembly in Epithelia of Drosophila. Curr. Biol. CB *30*, 4254-4262.e5.

Yang, K., Liu, M., Feng, Z., Rojas, M., Zhou, L., Ke, H., and Pastor-Pareja, J.C. (2021). ER exit sites in Drosophila display abundant ER-Golgi vesicles and pearled tubes but no megacarriers. Cell Rep. *36*.

Yano, H., Yamamoto-Hino, M., Abe, M., Kuwahara, R., Haraguchi, S., Kusaka, I., Awano, W., Kinoshita-Toyoda, A., Toyoda, H., and Goto, S. (2005). Distinct functional units of the Golgi complex in Drosophila cells. Proc Natl Acad Sci U A *102*, 13467–13472.

Yarwood, R., Hellicar, J., Woodman, P.G., and Lowe, M. (2020). Membrane trafficking in health and disease. Dis. Model. Mech. *13*, dmm043448.

Figure legends

Figure 1

A two-component system for controlling secretory protein trafficking *in vivo*.

(A) Principle of RUSH. A Streptavidin “hook” carrying an ER-retention signal is retained in the ER lumen and forms a complex with a secretory cargo protein tagged with a fluorescent protein and a Streptavidin-binding peptide (SBP), leading to ER retention of the cargo. Addition of biotin dissociates the hook-cargo complex, thus allowing cargo to exit the ER and synchronizing the passage of cargo through the secretory apparatus.

(B) Secretory cargo and ER-resident “hook” constructs. Cargo proteins consist of the N-terminal signal peptide and chitin-binding domain of Serpentine (Serp-CBD) fused to a Streptavidin-binding peptide (SBP) and a C-terminal EGFP (Serp-SBG, green) or mRFP (Serp-SBR, magenta) tag. ER-resident hook proteins consist of either core Streptavidin (SA) or Streptactin (ST) fused to an N-terminal signal peptide and a C-terminal KDEL sequence.

(C,D) Confocal sections of tracheal dorsal trunk (metamere seven) in living embryos expressing Serp-SBG (green) and palmitoylated mKate2 (palm-mKate2; magenta; C) or expressing Serp-SBR (magenta) and palmitoylated mNeonGreen (palm-mNeonGreen; green, D) in tracheal cells under the control of *btl*-Gal4. Anterior is to the left here and in all panels.

(E,F) Confocal sections of dorsal trunk in fixed embryos expressing Streptavidin-KDEL (SA-KDEL; magenta, E) or Streptactin (ST-KDEL; magenta, F) in tracheal cells, stained with antibodies against Streptavidin (E',F') and for chitin (tracheal lumen).

(G) Section of dorsal trunk in embryo expressing Streptactin-KDEL (magenta) stained with anti-Streptavidin and anti-KDEL antibodies, indicating localization of SA-KDEL in the ER.

Scale bar: (C-G), 5 µm.

Figure 2

The efficiency of ER retention depends on the ratio of cargo and hook proteins.

(A-E) Confocal sections of dorsal trunk in living embryos (stage 15) expressing Serp-SBG alone (control; A) or with one copy of SA-KDEL(weak) (B) or with the indicated number of copies of SA-KDEL(strong) (C-E) in tracheal cells. Note that the extent of ER retention of Serp-SBG in tracheal cells increases and luminal Serp-SBG levels decrease with increasing dosage of SA-KDEL.

(F) Quantification of the ratio of intracellular and luminal Serp-SBG signals. Number of embryos (n) is indicated. Each data point represents one embryo. Boxplot shows the median (line), interquartile range (box) and 1.5x interquartile range from the 25th and 75th percentile (whiskers). p-values (Student´s t-test) are indicated; n.s., not significant.

(G-H') Serp-SBG (green) was expressed under the control of the *ubiquitin* (*ubi*) promoter throughout wing imaginal discs of third-instar larvae and accumulates in the disc lumen. mCherry-nls (magenta) expressed under the control of *en*-Gal4 marks the posterior compartment in control discs (G). Expression of four copies of SA-KDEL in the posterior compartment leads to intracellular retention of Serp-SBG in SA-KDEL-expressing cells (H).

Scale bars: (A-E), 5 µm; (G,H), 50 µm.

Figure 3

Biotin injection triggers rapid ER exit and exocytosis of Serp-SBG in tracheal cells.

(A) Stills (maximum-intensity projections) from time-lapse movie of embryo (stage 15) expressing Serp-SBG and four copies of SA-KDEL in tracheal cells. After injection of biotin (1 mM) at t=0 min, Serp-SBG is released from the ER, accumulates at immobile puncta,

corresponding to ER exit sites, from 2 min onwards, and is subsequently secreted into the lumen. Fast-moving intracellular Serp-SBG-positive puncta, corresponding to endosomes, appear 15 min after injection (arrowheads, t=20 min). ROIs in tracheal cells (dashed white circle) and lumen (black circle) are indicated in top panel. Time (min:s) is indicated. See Movie S1.

(B) Confocal section of dorsal trunk in embryo (stage 15) expressing Serp-SBG, Rab4-mRFP and four copies of SA-KDEL in tracheal cells, 28 min after biotin injection. The recycling endosome marker Rab4-mRFP labels a subset of intracellular Serp-SBG puncta (arrowheads). Single-channel images display Serp-SBG and Rab4-mRFP intensities as a heat map. See Movie S2.

(C,C') Stills (maximum-intensity projections) of dorsal branch from time-lapse movie of embryo (stage 16) expressing Serp-SBG, Rab4-mRFP and four copies of SA-KDEL in tracheal cells. Time (min:s) is indicated. After injection of biotin at t=0 min, Serp-SBG is rapidly secreted into the lumen. At t=28 min, Serp-SBG is detectable in recycling endosomes marked by Rab4-mRFP (C', arrowheads). See movie S3.

(D) Quantification of Serp-SBG intensity in the lumen (black) and inside tracheal cells (grey) of dorsal trunk after biotin injection at t=0 min. Mean intensities +/- s.d., normalized to intensities at t=0 min, are shown. n=5 embryos.

Scale bars: (A,B,C,C'), 5 µm.

Figure 4

Rapid ER exit and passage of the Golgi apparatus by Serp-SBG.

(A) Stills from time-lapse movie of tracheal dorsal trunk in embryo (stage 15) expressing Serp-SBG, mCherry-Sec24 and four copies of SA-KDEL in tracheal cells. Biotin was injected at t=0 min. Serp-SBG (green) accumulates at ER exit-sites (mCherry-Sec24, magenta) at t=6:42. Time (min:s) is indicated. See Movie S5.

(B) Quantification of Serp-SBG signals at mCherry-Sec24-positive ERES. Each thin line indicates the mean of Serp-SBG intensity of at least 26 ERES per time point in one embryo, thick black line shows the mean of seven embryos. Data were normalized to mean intensities at the first time point. Serp-SBG accumulation at ERES is maximal seven minutes after biotin injection.

(C) Quantification of Serp-SBG levels at ten ERES distributed from apical (1) to basal (10) in tracheal cells indicates similar profiles of Serp-SBG trafficking.

(D) High-resolution images showing Serp-SBG (green) at a single mCherry-Sec24-labeled ERES (magenta) after biotin injection at t=0 min. After ER release, Serp-SBG colocalizes with mCherry-Sec24 (t=2:12) and subsequently shifts next to the mCherry-Sec24-marked ERES, presumably residing in the Golgi apparatus (t=3:48, 11:48), before disappearing from the ERES-Golgi complex (t=23:18). Images were processed using deconvolution. See Movie S6. Scheme (bottom panel) illustrates passage of Serp-SBG (green) through the ERES (magenta) and Golgi apparatus (grey).

(E) Quantification of the area of intersection between Serp-SBG and mCherry-Sec24. Each data point represents the mean +/- s.d. of the overlapping area between Serp-SBG and mCherry-Sec24 signals. Between 38 and 58 mCherry-Sec24-positive ERES were analyzed per time point. The black curve shows a local polynomial regression fit.

Scale bars: (A), 10 µm, insets: 2 µm; (D) 1 µm.

Figure 5

Manipulation of endogenous Fasciclin 2 protein *in vivo* and in cultured ovaries.

(A) Scheme of Fasciclin 2 (Fas2) protein (top) tagged with venus-YFP (green) flanked by StrepII tags (orange). The *fas2* locus encodes multiple transmembrane and GPI-linked isoforms, all of which carry the extracellular StrepII-venus-YFP-StrepII (SVS) tag. For simplicity, only a transmembrane isoform is shown. Streptactin-KDEL (bottom) mediates ER retention of secretory proteins carrying StrepII tags in their luminal (extracellular) portion.

(B,C) Epidermis in embryo (B) and third-instar larva (C) expressing Fas2::SVS (green). Two copies of Streptactin-KDEL and mCherry-nls (magenta) are co-expressed in epidermal stripes under the control of *en-Gal4*. While Fas2:SVS outlines lateral membranes of control cells, it accumulates in the ER of ST-KDEL-expressing cells marked by mCherry-nls.

(D,D') Wing imaginal disc of third-instar larva as in (B,C). Note retention of Fas2::SVS in the ER of cells in the posterior compartment. (D') shows close-up of the region marked by dashed square in (D).

(E,F) Confocal section of follicular epithelium in cultured ovarian follicles (stage 7) from *Fas2::SVS* females. Fas2::SVS localizes at lateral membranes in control egg chamber (E), but is retained in the ER in Streptactin-KDEL-expressing follicle cells (F).

(G) Stills from time-lapse movie of cultured egg chamber (stage 6) expressing Fas2::SVS (green in G) and two copies of Streptactin-KDEL in follicle cells. CellMask-orange (magenta) marks plasma membranes. After addition of biotin (at t=0 min; 1.5 mM final concentration) to the medium, Fas2::SVS is released from the ER, localizes in puncta (arrowheads) and becomes detectable at the plasma membrane 22 min after biotin addition. Time (min:s) is indicated. See Movie S10.

Scale bars: (B), 10 µm; (C,D), 50 µm; (D',E,F), 10 µm; (G), 5 µm.

Figure 6

Real-time analysis of tricellular junction assembly in the embryonic epidermis.

(A) Confocal projections of living embryo expressing endogenous Gli::SVS (green) and *ubi-*Dlg1::mTag-RFP (magenta). CyPET-nls (cyan) and two copies of ST-KDEL are expressed in epidermal stripes under the control of *hh-Gal4*. Note that Gli::SVS is retained in the ER of ST-KDEL-expressing cells (marked by CyPET-nls), whereas it accumulates at tricellular junctions in adjacent control cells. Close-ups show region marked by box in overview panels.

(B) Stills from time-lapse movie of embryo as in (A) injected with biotin at t=0 min. After release from the ER, Gli::SVS appears in ERES/Golgi puncta (t=5 min) and subsequently accumulates at tricellular junctions (t=12 min). Time (min:s) is indicated. See Movie S9.

(C) Cross-section of tricellular junctions of cells at boundary of hh-Gal4>ST-KDEL-expressing stripe in (B). After release from the ER, Gli::SVS first accumulates at tricellular junctions apically (white arrowheads). At tricellular junctions of non-ST-KDEL-expressing cells (left), Gli::SVS is distributed along the apical-basal extent of the vertex (open arrowhead).

(D) Quantification of Gli::SVS levels at tricellular junctions (TCJ, black) and inside cells (grey). Mean +/- s.d. and local polynomial regression fits (lines) are shown. n=4 embryos.

Scale bars: (A), 50 µm, close-ups: 10 µm; (B), 10 µm; (C), 5 µm.

Figure 7

ER retention of Notch::SVS causes cell fate specification defects resembling *N* loss-of-function mutants.

(A) Role of Notch signaling in tracheal tip cell specification. A single tip cell (orange) up-regulates expression of the Notch ligand Delta and stimulates Notch signaling in adjacent stalk cells (green), preventing these cells from adopting tip cell fate.

(B,C) Representative images of stage 15 *N::SVS*/+ control embryo (B) and *N::SVS*/+ embryo expressing two copies of ST-KDEL in tracheal cells (C) stained with anti-GFP (to detect N::SVS; green), anti-Dysfusion (Dysf; magenta) and anti-Streptavidin antibodies. Note weak N::SVS signals and a pair of Dysf-positive fusion cells at each tracheal metamere boundary in control embryo (B), whereas *btl*>ST-KDEL-expressing embryo shows intracellular retention of N::SVS and supernumerary Dysf-positive fusion cell nuclei (arrowheads in C).

(D,D') Live wing imaginal disc of *N::SVS*/+ third-instar larva expressing two copies of ST-KDEL and mCherry-nls in the posterior compartment under the control of *en-Gal4*. Note retention of N::SVS in the ER of posterior compartment cells marked by mCherry-nls. (D') shows a close-up of the boxed region at the compartment boundary in (D).

(E-G') Adult wings of control (*N::SVS*/+; E), N^1/+ (F) and *N::SVS*/+ flies expressing two copies of ST-KDEL under the control of *en-Gal4* (G). Note that retention of N::SVS in the posterior compartment leads to wing margin notches (arrowheads) and enlarged wing veins resembling the phenotype of N^1/+ mutants, but restricted to the posterior wing compartment. Close-ups (E',F',G') show enlarged view of distal L5 vein (boxed regions in (E-G). Anterior (A) and posterior (P) compartments and the compartment boundary (dashed line) are indicated in (F).

Scale bars: (B,C), 20 µm; (D), 50 µm; (D'), 10 µm; (E,F,G), 500 µm; (E',F',G'), 100 µm.

Figure 1

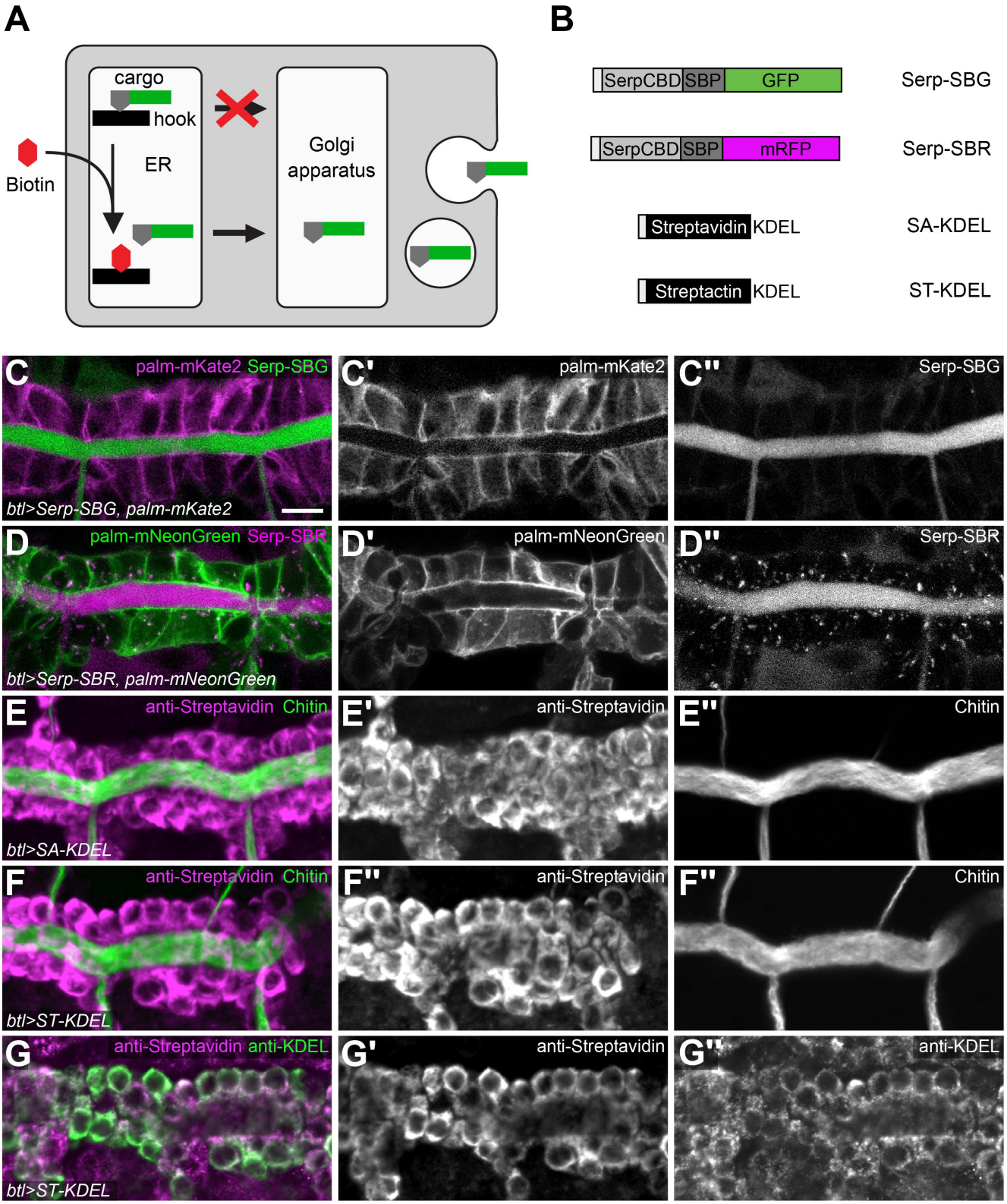
A
cargo
hook
ER
Biotin
Golgi apparatus
B
SerpCBD
SBP
GFP
Serp-SBG
SerpCBD
SBP
mRFP
Serp-SBR
Streptavidin
KDEL
SA-KDEL
Streptactin
KDEL
ST-KDEL
C
palm-mKate2 Serp-SBG
btl>Serp-SBG, palm-mKate2
C'
palm-mKate2
C''
Serp-SBG
D
palm-mNeonGreen Serp-SBR
btl>Serp-SBR, palm-mNeonGreen
D'
palm-mNeonGreen
D''
Serp-SBR
E
anti-Streptavidin Chitin
btl>SA-KDEL
E'
anti-Streptavidin
E''
Chitin
F
anti-Streptavidin Chitin
btl>ST-KDEL
F'
anti-Streptavidin
F''
Chitin
G
anti-Streptavidin anti-KDEL
btl>ST-KDEL
G'
anti-Streptavidin
G''
anti-KDEL

Figure 2

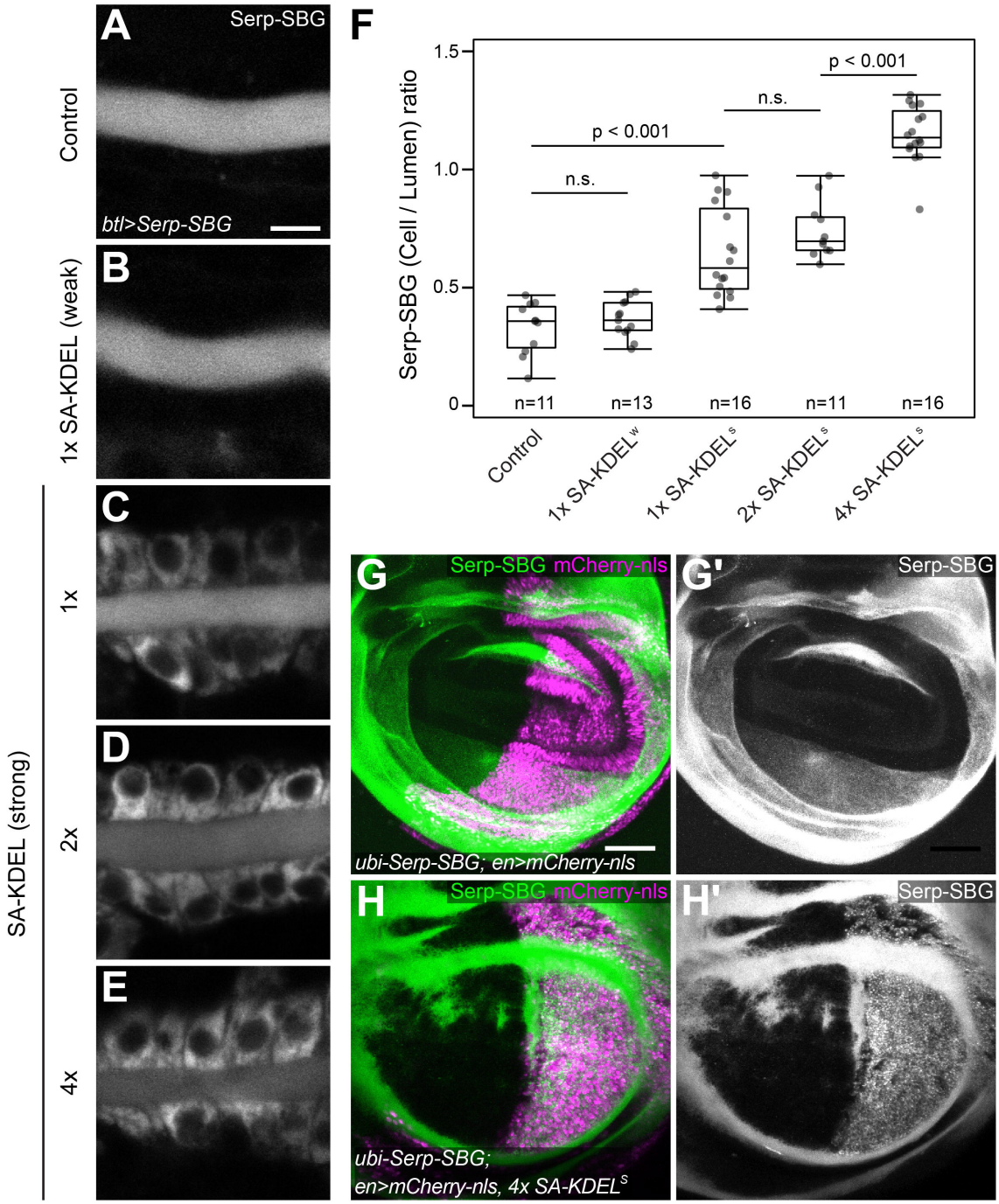
A
Serp-SBG
btl>Serp-SBG
Control
B
1x SA-KDEL (weak)
C
1x
D
2x
E
4x
SA-KDEL (strong)
F
Serp-SBG (Cell / Lumen) ratio
1.5
1.0
0.5
0
p < 0.001
n.s.
p < 0.001
n.s.
n=11
n=13
n=16
n=11
n=16
Control
1x SA-KDEL^w
1x SA-KDEL^s
2x SA-KDEL^s
4x SA-KDEL^s
G
Serp-SBG mCherry-nls
ubi-Serp-SBG; en>mCherry-nls
G'
Serp-SBG
H
Serp-SBG mCherry-nls
ubi-Serp-SBG;
en>mCherry-nls, 4x SA-KDEL^S
H'
Serp-SBG

Figure 3

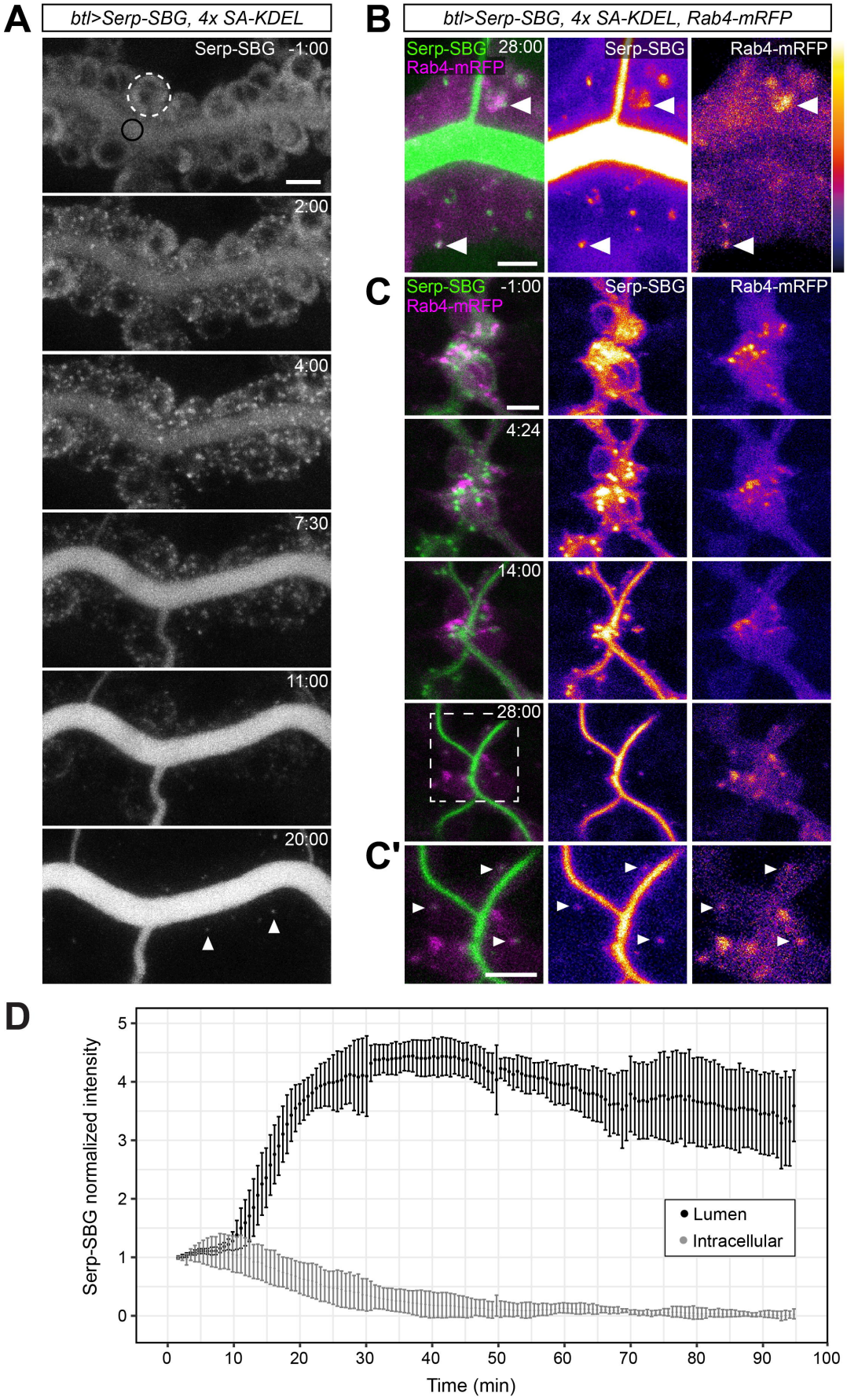
A
btl>Serp-SBG, 4x SA-KDEL
Serp-SBG -1:00
2:00
4:00
7:30
11:00
20:00
B
btl>Serp-SBG, 4x SA-KDEL, Rab4-mRFP
Serp-SBG 28:00
Rab4-mRFP
Serp-SBG
Rab4-mRFP
C
Serp-SBG -1:00
Rab4-mRFP
Serp-SBG
Rab4-mRFP
4:24
14:00
28:00
C'
D
Serp-SBG normalized intensity
Time (min)
Lumen
Intracellular
0
1
2
3
4
5
0
10
20
30
40
50
60
70
80
90
100

Figure 4

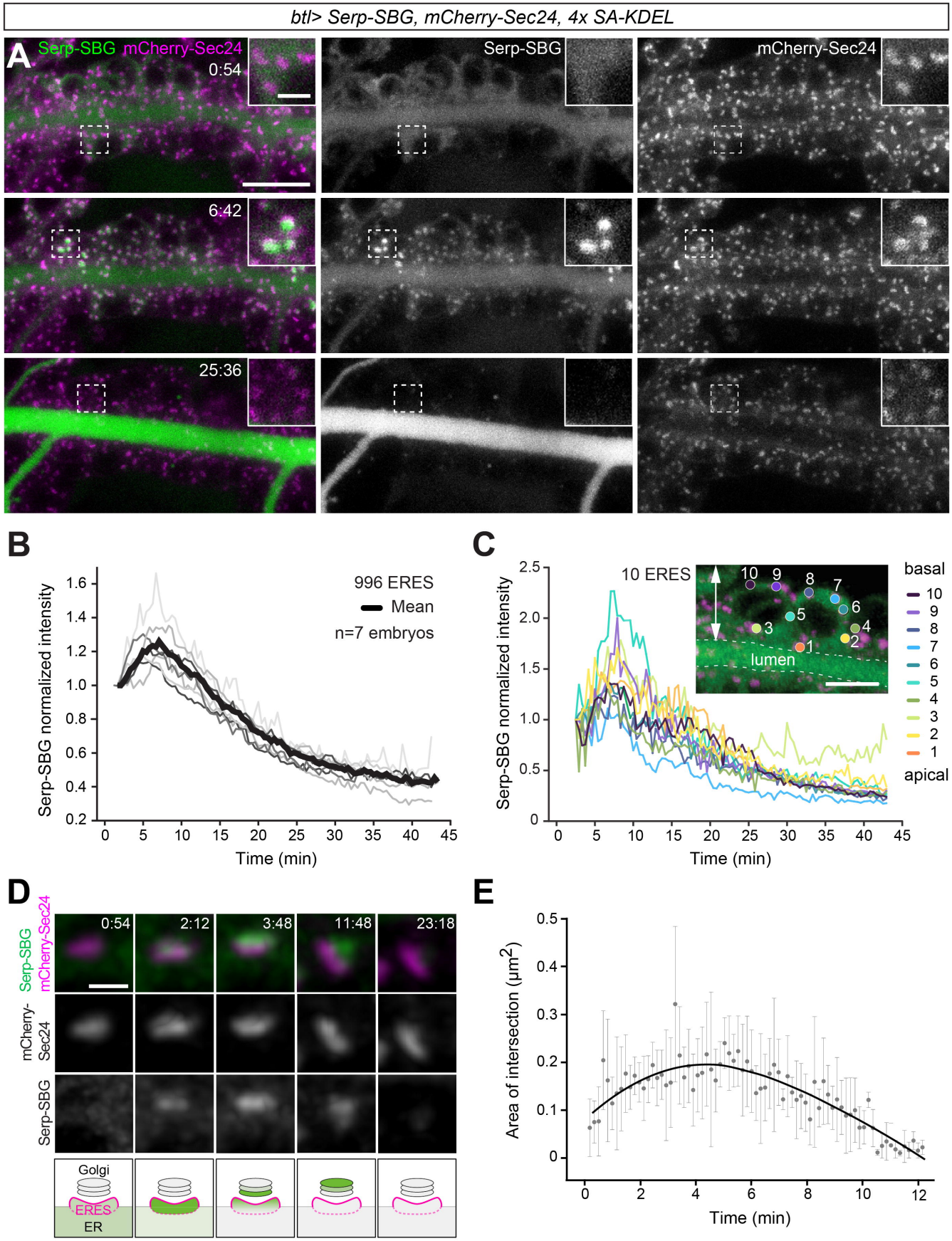
btl> Serp-SBG, mCherry-Sec24, 4x SA-KDEL
A
Serp-SBG mCherry-Sec24
0:54
6:42
25:36
Serp-SBG
mCherry-Sec24
B
996 ERES
Mean
n=7 embryos
Serp-SBG normalized intensity
Time (min)
C
10 ERES
lumen
basal
apical
Serp-SBG normalized intensity
Time (min)
D
0:54
2:12
3:48
11:48
23:18
Serp-SBG
mCherry-Sec24
mCherry-Sec24
Serp-SBG
Golgi
ERES
ER
E
Area of intersection (μm2)
Time (min)

Figure 5

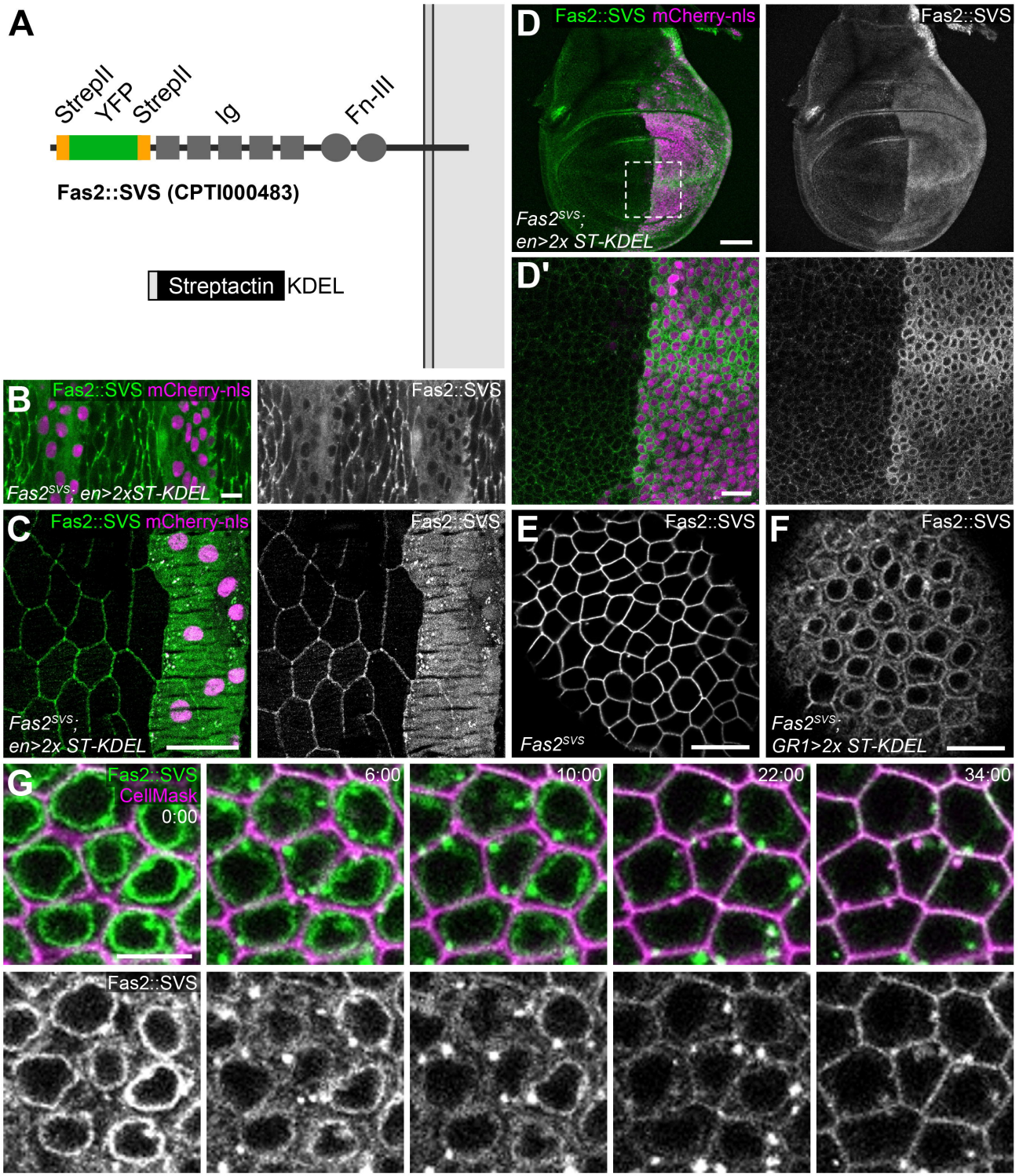
A
StrepII
YFP
StrepII
Ig
Fn-III
Fas2::SVS (CPTI000483)
Streptactin
KDEL
B
Fas2::SVS mCherry-nls
Fas2::SVS
Fas2SVS; en>2xST-KDEL
C
Fas2::SVS mCherry-nls
Fas2::SVS
Fas2SVS; en>2x ST-KDEL
D
Fas2::SVS mCherry-nls
Fas2::SVS
Fas2SVS; en>2x ST-KDEL
D'
E
Fas2::SVS
Fas2SVS
F
Fas2::SVS
Fas2SVS; GR1>2x ST-KDEL
G
Fas2::SVS
CellMask
0:00
6:00
10:00
22:00
34:00
Fas2::SVS

Figure 6

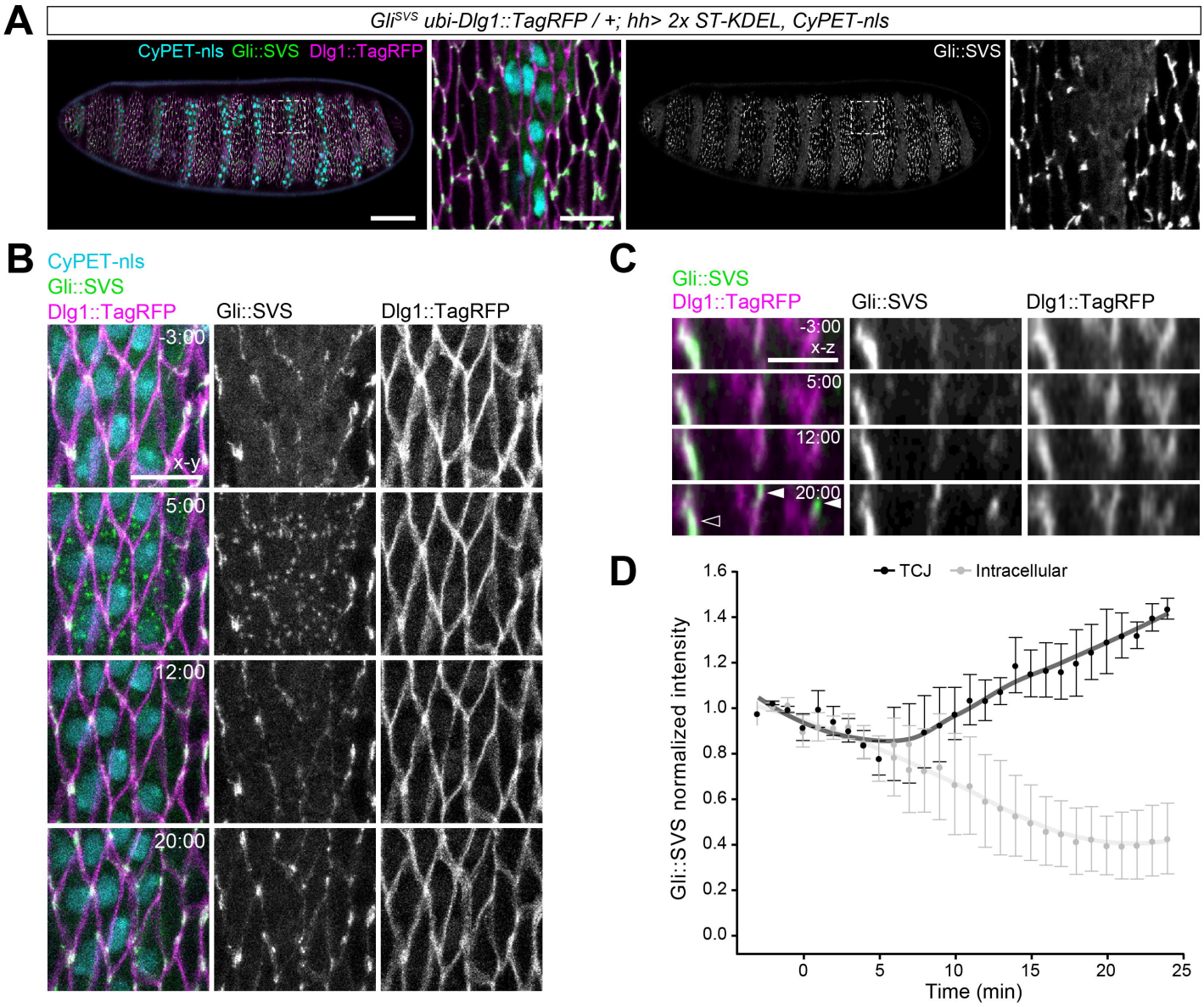
A
Gli^SVS ubi-Dlg1::TagRFP / +; hh> 2x ST-KDEL, CyPET-nls
CyPET-nls Gli::SVS Dlg1::TagRFP
Gli::SVS
B
CyPET-nls
Gli::SVS
Dlg1::TagRFP
Gli::SVS
Dlg1::TagRFP
-3:00
x-y
5:00
12:00
20:00
C
Gli::SVS
Dlg1::TagRFP
Gli::SVS
Dlg1::TagRFP
-3:00
x-z
5:00
12:00
20:00
D
TCJ
Intracellular
Gli::SVS normalized intensity
1.6
1.4
1.2
1.0
0.8
0.6
0.4
0.2
0.0
0
5
10
15
20
25
Time (min)

Figure 7

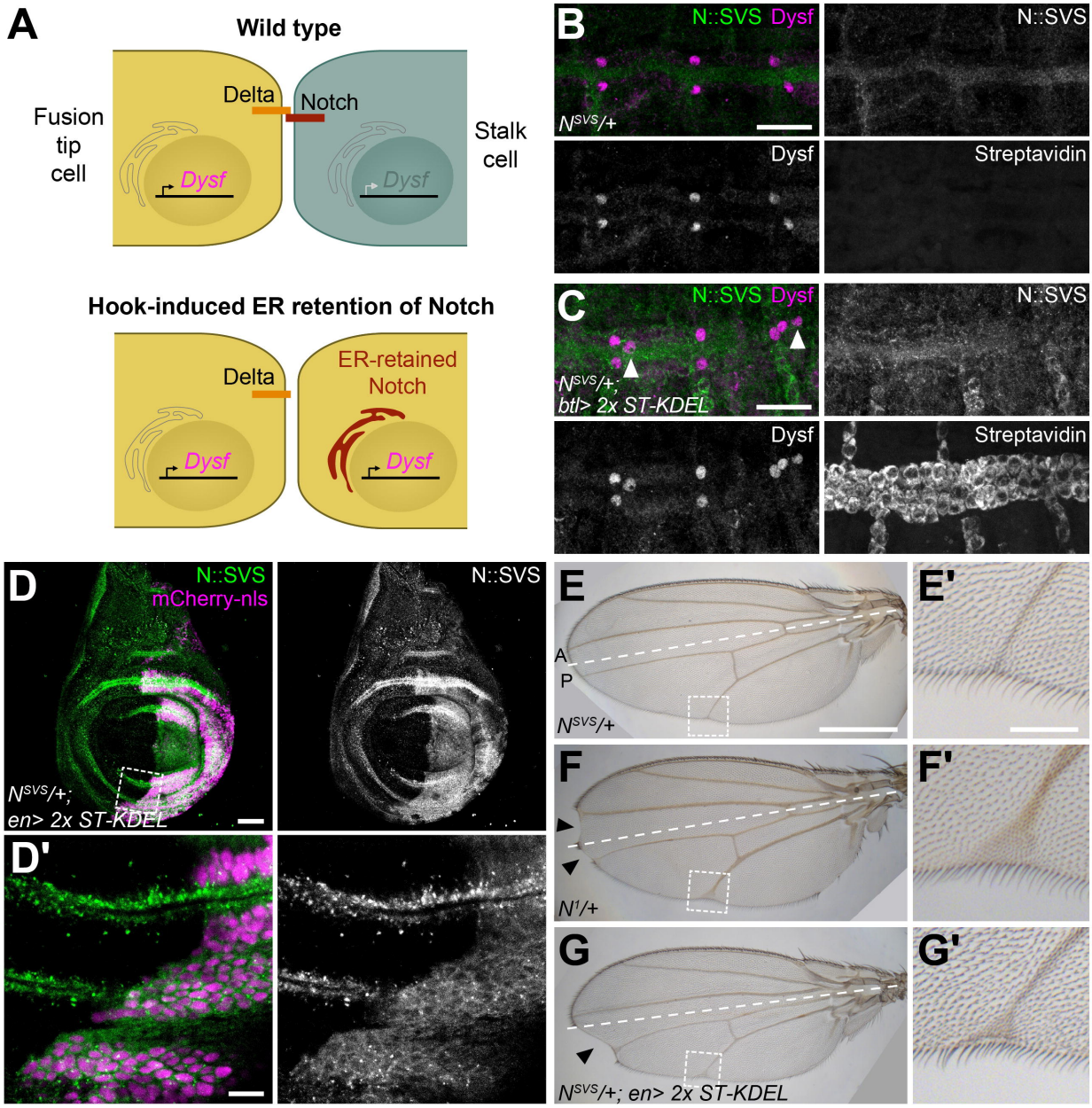
A
Wild type
Fusion tip cell
Delta
Notch
Stalk cell
Dysf
Dysf
Hook-induced ER retention of Notch
Delta
ER-retained Notch
Dysf
Dysf
B
N::SVS Dysf
N::SVS
N^{SVS}/+
Dysf
Streptavidin
C
N::SVS Dysf
N::SVS
N^{SVS}/+; btl> 2x ST-KDEL
Dysf
Streptavidin
D
N::SVS mCherry-nls
N::SVS
N^{SVS}/+; en> 2x ST-KDEL
D'
E
E'
A
P
N^{SVS}/+
F
F'
N^{1}/+
G
G'
N^{SVS}/+; en> 2x ST-KDEL